ADVANCED ENERGY MATERIALS
www.advenergymat.de

Achieving a Large Driving Force on Triboelectric Nanogenerator by Wave-Driven Linkage Mechanism for Harvesting Blue Energy toward Marine Environment Monitoring

Jiajia Han, Yuan Liu, Yawei Feng, Tao Jiang, and Zhong Lin Wang**

Water wave energy is regarded to be a promising renewable energy source to relieve the pressure of fossil energy shortage and achieve a sustainable future. A cylindrical wave-driven linkage mechanism triboelectric nanogenerator (WLM-TENG) with unidirectional rotation is designed and fabricated to effectively harvest water wave energy. The enormous force generated by water waves, which is up to 424.3 N m^{-2}, is used to drive the TENG through its simple and smart mechanical structure. This force allows the rotor to overcome the large resistance caused by the full contact between rabbit furs and electrodes. The output current can reach about 30 μA and the output power arrives at 50 mW. Moreover, self-powered applications powered by the WLM-TENG are successfully demonstrated, including indicating light-emitting diodes (LEDs), multifunctional barometer, portable anemometer, and multifunctional water quality detection pen. This work renders an effective approach to harness the enormous force generated by the water waves, enhancing the water wave energy harvesting ability of the TENG, toward practical applications of marine environment monitoring.

1. Introduction

Electric power is an indispensable energy that plays an important role in today's society.[1] Nonrenewable energy sources, such as fossil fuels,[2] which are mainly used to generate electricity, are currently facing a serious problem of depleted reserves.[3] Meanwhile, the consequence of greenhouse gases exhausted by fossil fuel combustion around the world is also an urgent problem to be solved.[4–7] The resulting increase in the price of energy fuels and stricter environmental regulations also have great impacts on the social developments. Based on these, great efforts have been made to seek alternative clean energy sources. Water wave energy, as one of the most promising energy sources in the natural environment,[8–10] offers opportunities to relieve the pressure of exhausted fossil energy reserves due to its wide distribution, huge amount, clean and renewable characteristics.[11–13] Most wave converters rely on electromagnetic generators, which exhibit the problems of high construction and maintenance costs, low energy conversion efficiency at low frequency, poor reliability and stability in wave energy collection, limiting the large-scale applications and developments.[9,14]

Triboelectric nanogenerator (TENG, also called as Wang generator), by coupling the effects of triboelectrification and electrostatic induction,[15–18] is an emerging mechanical energy harvesting approach, showing obvious advantages of high power density, light weight, low fabrication cost and good low-frequency adaption for wave energy collection. Several structural designs of TENG devices have been carried out to harvest water wave energy,[19,20] including the spring-assisted or internal swing structure. For example, a spherical TENG assisted with a spring can harvest multidirectional water wave energy,[21–23] and a swing-structured TENG can realize the harvesting of ultra-low-frequency water wave energy.[24–26] Actually, the pendulum-like operation mode of the TENG has been verified to be an effective strategy to enhancing the output frequency and energy conversion efficiency for wave energy harvesting.[27,28] However, for such working mode, the gap between the pendulum component and the stator leads to the decrease of the transferred charges to a certain extent, and additional charge supplement is required. And the motion of this structure depends excessively on the amplitude of the waves, the smoothness of the bearing, and the gap between the pendulum and the stator. Besides, these existing wave energy harvesting devices usually interact directly with the water waves, but the huge force of water waves cannot be fully utilized due to the lacking of effective power transmission mechanism. On this basis, we try to improve the power transmission

J. Han, Y. Liu, Y. Feng, T. Jiang, Z. L. Wang
CAS Center for Excellence in Nanoscience
Beijing Key Laboratory of Micro-Nano Energy and Sensor
Beijing Institute of Nanoenergy and Nanosystems
Chinese Academy of Sciences
Beijing 101400, P. R. China
E-mail: jiangtao@binn.cas.cn; zlwang@gatech.edu
J. Han, T. Jiang
School of Nanoscience and Technology
University of Chinese Academy of Sciences
Beijing 100049, P. R. China
Z. L. Wang
Georgia Institute of Technology
Atlanta, GA 30332-0245, USA

The ORCID identification number(s) for the author(s) of this article can be found under https://doi.org/10.1002/aenm.202203219.

DOI: 10.1002/aenm.202203219

structure of TENG to effectively utilize the wave force and capture more energy from the water wave motions, thereby providing possible solution to achieving higher performance.

In addition, the selection of triboelectric materials also has a great influence on the output performance and lifetime of TENGs. When two materials with different polarities are in contact, an equal amount of electrostatic charges with opposite signs will appear on their surfaces. In previous works, the soft contact mode using the rabbit fur materials was adopted to enhance the device performance,[29–32] in which the gap between the rabbit furs and electrodes greatly affects the electrical outputs of the TENG. The decrease of the gap can improve the effective contact between them and raise the transferred charge amount, but it also increases the frictional resistance so that a larger driving force is required to drive the rotor. Therefore, a simple structure TENG that can provide large driving force for the rotor to rotate is desirable, for example, using a linkage mechanism to transmit the huge wave forces to the rabbit fur-based rotor.

In this work, a cylindrical wave-driven linkage mechanism TENG (WLM-TENG) was fabricated to harvest water wave energy. The waves lift the floating board to move vertically and convert the motion into a circular motion of the rotor through a simple mechanical structure, so the enormous force generated by the water waves drives the movement of the rotor. The potential energy of waves is transformed into the kinetic energy of the rotor, which is further converted into electrical energy by triboelectrification. The rotor overcomes the resistance caused by the full contact between rabbit furs and electrodes, and the peak short-circuit current could reach about 30 μA. The peak power and average power reached 50 and 2.99 mW, respectively. Finally, a self-powered environmental detection system powered by the WLM-TENG was demonstrated, including indicating light emitting diodes (LEDs), multifunctional barometer, portable anemometer and multifunctional water quality detection pen. This work proposed a new TENG structure for effective water wave harvesting toward large-scale blue energy.

2. Results and Discussion

2.1. Device Structure and Working Principle

Figure 1a illustrates the designed wave-driven linkage mechanism cylindrical TENG (WLM-TENG). Its normal operation is based on a power transmission chain and a swing-to-rotation accessory. Our power generation unit is fixed above the water

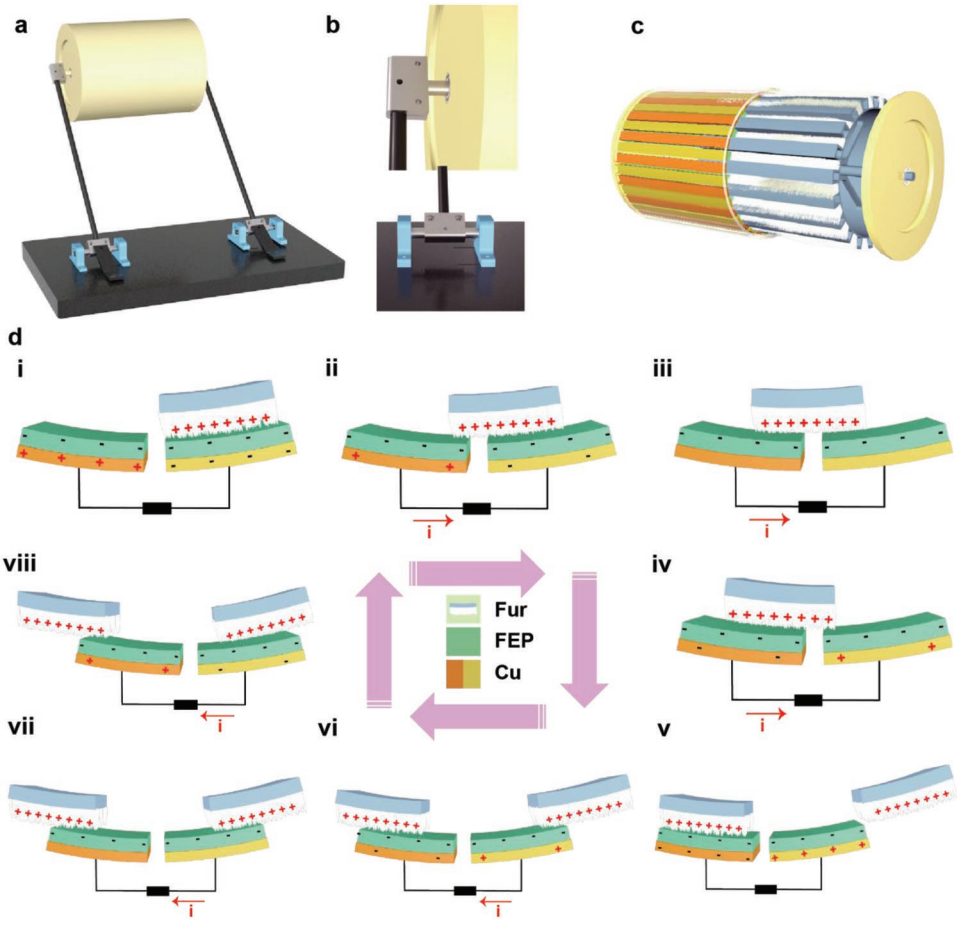

Figure 1. Schematic diagrams showing the structure and working principle of the WLM-TENG. a–c) Structural design of the WLM-TENG, including the structures of whole device with a linkage mechanism, T-shape connectors, and cylindrical rotor and stator. d) Sketches of the eight states in one full electricity-generating cycle, focusing on the charge distributions at the two sector-electrodes.

surface, so that the rotor can be twirled under the interaction of water waves and power transmission chain. The power transmission chain is a simple linkage mechanism, which converts the mechanical energy of water waves into the kinetic energy of the rotor. As depicted in Figure 1b, the rotor of the TENG and a floating plate are connected by T-shape connectors.

The floating board is made up of a piece of foam and a carbon fiber board, which is set upon the water surface to harvest the impact energy from water. The foam board is applied to float the carbon fiber plate. While in the real marine environment, the corrosion of foam and the impact of hazardous substances produced after decomposition on the marine ecological environment make it unsuitable for practical applications. Hence, the foam plate can be replaced by other corrosion resistant materials such as hollow carbon fiber box.

Under the combined action of the T-connectors and ceramic bearings, the impact of water waves can cause a circular motion of the TENG rotor. For the fabricated TENG, a gear-like cylinder printed by UV-curing resins or polylactic acid plastics serves as the rotor. The cylinder has a hollow structure that can reduce the weight of the rotor (Figure S1a, Supporting Information). And the rabbit furs are attached to the grooves with a depth of 10 mm. For the stator part, customized flexible printed circuit (FPC) boards are firstly covered with 38-grid fluorinated ethylene propylene (FEP) thin films. After rolled into a round roll, they were attached to the inner wall of the shell. This configuration is presented in Figure S1b (Supporting Information). The designed WLM-TENG is centrosymmetric as a whole, both in terms of the layout and weight and it is able to achieve continuous rotation, rather than the swing motion, by means of a one-way bearing fixed on the central shaft of the rotor. The structural detail photographs of the device are displayed in Figure S1c–e (Supporting Information).

According to our previous work, soft-contact mode TENGs could achieve higher output performance for the enhanced surface charge density provided by the applied positive fur brushes. The power generation of the fabricated TENG is mainly based on the triboelectrification and electrostatic induction between different materials. During the rotation process of the rotor under external mechanical triggering, opposite net electrostatic charges can be accumulated on the FEP films and the strip-shaped rabbit fur brushes until the saturated state. Under the saturated state, the amount of positive charges on the fur brushes is equal to the amount of negative charges on the FEP films. But the charge density on the fur brushes is the double of that on the FEP for the half area. The charge accumulation process of the WLM-TENG at the short-circuit state (Q_{SC}) is shown in Figure S2a (Supporting Information). The surface charges on the FEP films get saturated to 1100 nC after 1100 s of continuous external mechanical stimulations (Figure S2b, Supporting Information).

The working principle of the WLM-TENG is illustrated in Figure 1d. When the rotor is stimulated mechanically, the rabbit furs revolve skimming the FEP films of the stator, and the electrons transfer from the ordinary fur brushes to the FEP films due to the triboelectrification. At the initial state (state i), the brush is placed exactly above the right electrode. The negative free charges are induced on the right electrode to shield the excessive positive-polarization above it. When the fur rotor rotates clockwise relative to the stationary electrodes (states i-v), the intensity of positive-polarization above the right electrode decreases, while that above the left electrode increases. As a result, the free charges on the two electrodes will be redistributed due to the electron transfer from the right electrode to the left one, generating a current flow across the external circuit. After the fur rotor further rotates to pass through the left electrode (states v-viii), the electrons flow back to the right electrode, generating a reverse current pulse across the external resistor. The constant rotation produces continuous alternating-current (AC) outputs of the WLM-TENG.

2.2. Performance Optimization of the WLM-TENG

The output performance of the fabricated device was quantitatively characterized in a standard wave tank. In the water tank, the wave generator located at the end of the tank and was accurately controlled to obtain water waves with aimed parameters (**Figure 2**a). The main body of the TENG (yellow cylinder) was placed on a customized 3D-printed holder in order to separate from the water. In practical applications, the encapsulated TENG can be anchored to the coast or on ships. According to the characteristic of the mechanical structure, the floating plate rises up to a certain height and then falls back to the original position under the undulation of the waves. The utilization of the limit plate is to control the lifting state of the floating plate, preventing too large inclination angle (vertical to the water surface). As for the motion mode of the rotor in the WLM-TENG, two different modes of rotor rotation and swing were realized by installing different bearings at the central shaft (Figure 2b,c). Installing common bearings on the rotating shaft can cause the swing motion of the rotor, while installing unidirectional bearings can lead to a circular motion.

Figure 2d–f presents the comparison of transferred charge (Q_{SC}), short-circuit current (I_{SC}) and open-circuit voltage (V_{OC}) of the WLM-TENGs using different bearings under the same condition of water wave stimulations (1.0 Hz). It is obvious that the outputs at the rotation-mode are much greater than those at the swing-mode. That is because the floating board is lifted at a limited height and falls quickly with the waves. When the rotor is subjected to the force from the floating plate, the rotation direction of the rotor is rapidly switched in the case of using ordinary bearings. However, the rabbit furs on the rotor do not have enough time to change the direction of movement, which will generate large frictional resistance during the movement. Therefore, no effective relative position change between the triboelectric materials occurs, resulting in the reduced output performance of the device. When the ordinary bearings at the center of the rotor are replaced by one-way bearings, the rotor revolves in one direction under the action of the central shaft. Effective relative displacement is slowly generated between the rabbit furs and FEP films, so relatively higher outputs can be achieved. For the rotation-mode, the TENG can generate the maximum voltage of 3.0 kV, maximum current of 20 μA, and maximum transferred charge of 1100 nC.

Subsequently, the influence of water wave frequency on the TENG outputs was investigated at the outer diameter of 150 mm for the rotor and the rabbit fur strip number of 19, as shown in Figure 2g–i. The frequency can be adjusted by varying the dwell time of the wave generator in the water wave tank. When the

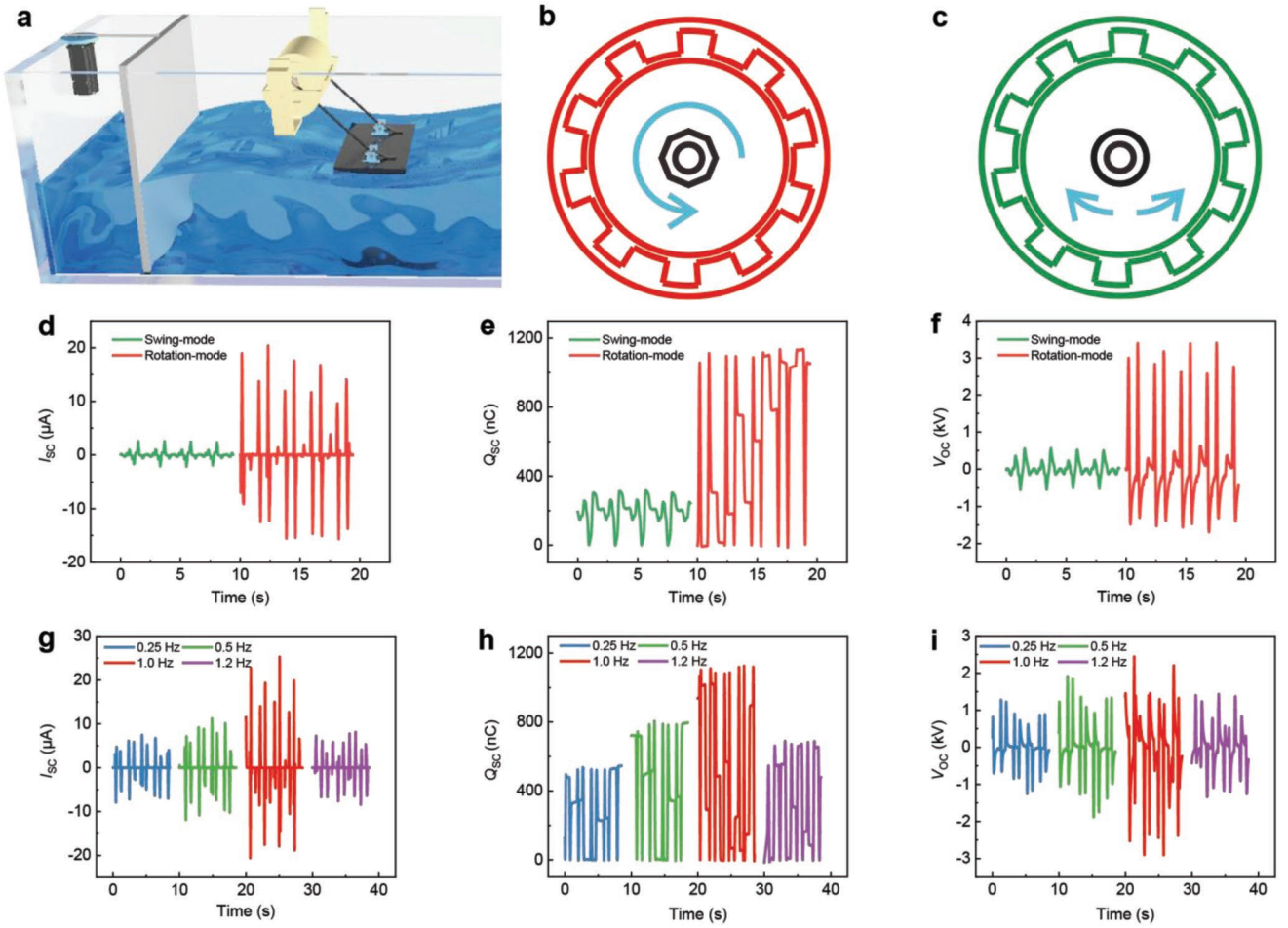

Figure 2. Influences of internal structure and water wave frequency on the output performance of TENG. a) Schematic diagram of the standard wave tank and the measurement method of the WLM-TENG. b,c) Comparison of two working modes: swing-mode and rotation-mode. d–f) Output performance of the TENG in the two working modes, including I_{SC}, Q_{SC}, and V_{OC}. g–i) Waveforms of the electrical outputs for the rotation-mode TENG at different wave frequencies.

water wave frequency is 1.0 Hz, the WLM-TENG can obtain the best output performance. If the frequency is higher than 1.0 Hz (e.g., 1.2 Hz), the output will drop slightly. This may be because that the floating plate is lifted again under the action of the next wave before it falls to its original position under one wave triggering, leading to the reduction of the moving distance and corresponding rotation angle of the rotor. As the water wave frequency decreases, the device motion frequency also decreases, which will lower the output performance. When the frequency is in the range of 0.4–1.0 Hz, the rotation-mode can still achieve higher performance than the swing-mode (Figure S3, Supporting Information), and the outputs increase with increasing the frequency. Hence, the following tests were carried out at the water wave frequency of 1.0 Hz.

Besides the motion mode and water wave condition, the structural parameters influencing the output performance were also optimized, as presented in **Figure 3**. The simplified schematic diagram of the motion mechanism of the floating plate and rotor is shown in Figure 3a. When the floating plate is lifted by the same height, the rotation angle α of the rotor is negatively correlated with the length l of connecting rod, which can be approximately calculated as:

$$\sin\frac{\alpha}{2}=\frac{h}{2l} \tag{1}$$

The rotation angle α should not exceed 180°, because the floating plate needs to perform continuous reciprocating motion in the vertical direction. In the effective range of α, with the decrease of l, the value of $\sin\frac{\alpha}{2}$ will increase, and the corresponding α will also increase. This is beneficial to increase the output performance of the device. The length of connecting rod has a great influence on the output frequency of the I_{SC}, Q_{SC}, and V_{OC} as shown in Figure 3b. The electrode-grid number was chosen as 38, and the gap between the rotor and the shell was set as 5 mm. When the water depth is fixed at 45 cm and the length of connecting rod is 25 cm, the floating plate can just touch the water surface. If a connecting rod of 20 cm is used, the floating plate will only partially touch the water surface, as shown in Figure S4 (Supporting Information). Therefore, the shortest connecting rod length should be selected according to the height from the water surface to obtain the optimal output performance in practical applications.

Then the dependence of the output performance of the TENG on the grid number of the electrodes was studied, as

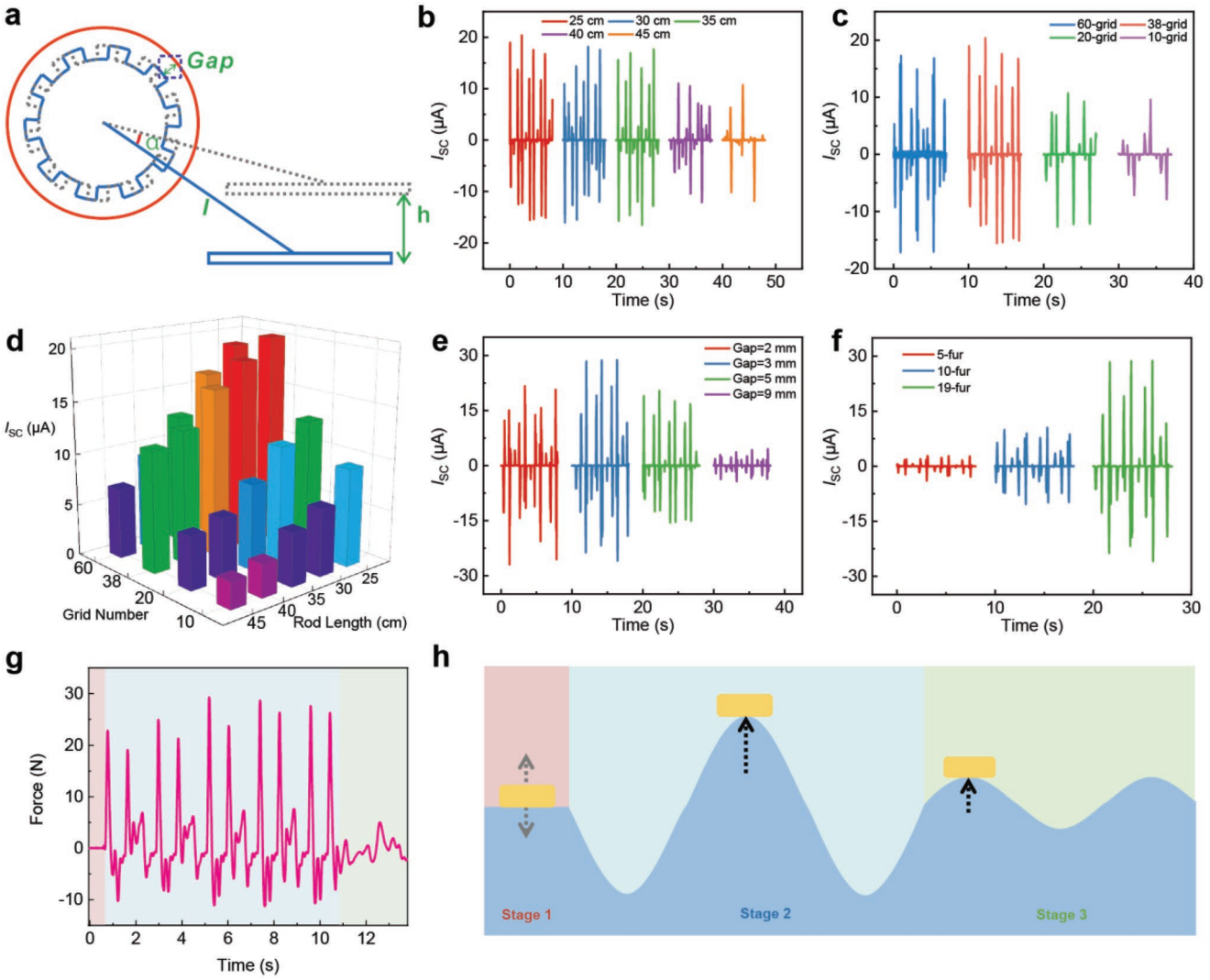

Figure 3. Structural optimization of the WLM-TENG. a) Schematic diagrams of the connecting rod and internal motion mechanism of the WLM-TENG. b–d) The trends of I_{SC} of the WLM-TENG for different lengths of connecting rod and different grids. e) The I_{SC} outputs at different gaps between the rabbit furs and electrodes. f) The I_{SC} for various numbers of the rabbit fur strips at the same electrode width. g) The force from the undulation of waves exerted on the floating board, when the frequency of water waves is 1 Hz (Symbol represents the direction of force, positive in orientation). h) Simplified force state diagram of floating board.

shown in Figure 3c, using a connecting rod length of 25 cm and a rotor-shell gap of 5 mm. It is apparent that under the same external conditions, the electrodes with more grids can generate higher current output. But when the grid number of electrodes increases to 60, the strip number of rabbit furs is 30, and the frictional resistance also increases. Under this stimulated condition, the force provided by the water waves is not sufficient to drive the rotor to rotate normally, so the output performance decreases slightly. Figure 3d summarizes the effects of the connecting rod length and electrode grid number on the current of the WLM-TENG, indicating that the 38-grid electrode and the shortest connecting rods are favorable under the performed conditions. So, we selected the configuration of 38-grid electrode and 25 cm-long connecting rod in the following experiments.

After these, we adjusted the gap between the rotor and the shell in order to change the contact tightness between the rabbit furs and FEP films. The gap in this case refers to the distance between the outer diameter of the rotor and the inner diameter of the shell (Figure 3a). It is well known that the frictional resistance increases as the distance between the rabbit furs and FEP films decreases. Among several gap distances we set (2, 3, 5, and 9 mm), the best output was obtained at the gap of 3 mm (Figure 3e). When the gap is reduced to 2 mm, the rotor movement is hindered and the current output decreases, due to the excessive frictional resistance. The corresponding Q_{SC} and V_{OC} profiles are shown in Figures S5 and S6 (Supporting Information).

In addition, we also explored the influence of the number of rabbit fur strips on the output performance, when keeping the number of electrode grids unchanged (the rotor-shell gap is 3 mm). The size of each rabbit fur strip remains the same as above, but the number of strips attached on the rotor varies from 19 to 5. Clearly, the peak values of the I_{SC}, Q_{SC}, and V_{OC}

all decrease with decreasing the fur strip number (Figure 3f and Figure S6, Supporting Information). Different from previous cylindrical TENGs with a few rabbit furs for charge supplement, in this work, the rabbit furs were used as the friction materials. Only when the number of rabbit fur strips is half of the electrode number can the maximum charge transfer be achieved. The decrease in the fur strip number will lead to no charge transfer at the positions corresponding to the empty grooves on the rotor, thereby resulting in lower outputs.

Subsequently, the force generated by the water waves was quantified by a commonly used force transducer. The upward force of the water waves on the floating board within 10 s was tested, when the frequency of water waves was set as 1 Hz, and the wave height is 10 cm (Figure 3g). The variation of curve corresponds to three stages of water wave motion, as shown in Figure 3h. In the first stage, the water is in a static state. In this case, the gravity of the floating board is equal to the buoyancy of the water, and the floating board is stationary on the water surface. When it comes to stage 2, the wave generator is working. In addition to the gravity and buoyancy, the water wave fluctuations provide an additional upward thrust to the floating board. The huge force, up to 29.7 N, is transmitted to the rotor through the connecting rod structure, driving the rotor to overcome the frictional resistance between the rabbit fur and the stator. The area of floating board is 0.07 m^2 and the pressure can reach 424.3 N m^{-2}. When the wave generator stops working, the water waves don't stop moving in an instant (stage 3). The floating board continues to rise and fall for a period under the action of residual waves until the water surface calms down. Note that due to the floating plate structure, the total wave energy-to-mechanical energy conversion efficiency for the WLM-TENG can reach 65.3% (Note S1, Supporting Information), which is much larger than that of the state-of-art TENGs.

Furthermore, the electrical outputs of the WLM-TENG when loading an external resistor were also characterized. The peak current-resistance and peak voltage-resistance relationships for the rotation-mode and swing-mode are depicted in **Figure 4**a. The instantaneous output voltage is calculated by

$$V = I_t R \tag{2}$$

where R is the loaded resistance and I_t is the instantaneous current across the resistance. The output power of the two motion modes is illustrated in Figure 4b. The average power of the TENG can be obtained by

$$P_{ave} = \frac{W}{T} = \int_0^T I_t^2 \, R \, dt / T \tag{3}$$

where T is the operation duration of the cylindrical TENG. For the rotation-mode, the instantaneous peak power reaches its maximum value of 50 mW, and the average power is about 2.99 mW at the matched resistance of 200 MΩ, respectively. According to the device volume, the corresponding peak power

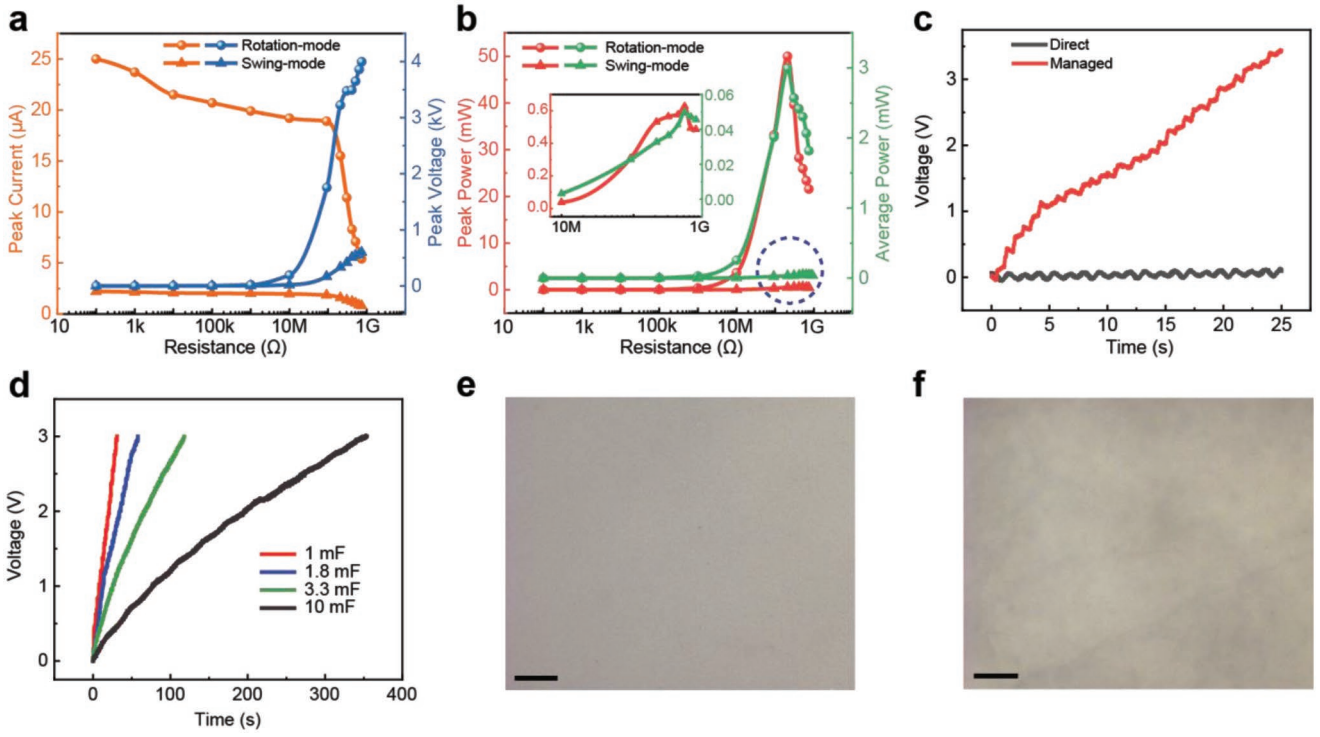

Figure 4. Output performance, charging performance, and durability tests of the WLM-TENG. a) Comparison of instantaneous peak current and peak voltage for the WLM-TENG when loading different resistances at the rotation-mode and swing-mode. b) Comparison of the peak power and average power-resistance relationships for the WLM-TENG at the rotation-mode and swing-mode. Inset: Enlarged view of the curve marked. c) Charging voltage curve of a 1 mF capacitor by the WLM-TENG with or without the power management circuit. d) Charging voltage on various capacitors for the rotation-mode WLM-TENG integrated with the power management circuit. Optical microscope morphologies of the FEP films e) before and f) after all of the tests. The scale bars in (e) and (f) represent 10 μm.

density is 14.1 W m^{-3}. However, the peak power for the rotation mode is only 0.57 mW, and the average power is only 0.05 mW when the loaded resistance is 500 MΩ. That verifies the higher output energy of the rotation-mode TENG than the swing-mode one again. In addition, at the lower frequency of 0.25 Hz in the standard wave tank, the average power of TENG is 0.113 mW and its average power density is 0.032 W m^{-3}.

For promoting the application of TENG in harvesting water wave energy, an efficient and matched power management circuit was implemented, as schematically shown in Figure S8a (Supporting Information). Figure 4c shows the comparison of the charging capability of the TENG device to a capacitor of 1 mF with or without the power management circuit. And the charging speed to the capacitor is greatly improved after the power management on the power output from the TENG. The voltage on the 1 mF capacitor can arrive at 3.5 V in 25 s. Regarding the working mode, the rotation-mode TENG has the higher charging performance to the capacitor than the swing-mode TENG, due to the higher electrical outputs (Figure S8b, Supporting Information). For different capacitors of 1, 1.8, 3.3, and 10 mF charged by the rotation-mode TENG, the time for the voltage to reach 3.0 V is 22, 58, 117, and 352 s, respectively (Figure 4d). The wear of FEP film and rabbit fur was also characterized after all of the data acquisition, including structural optimization, output power, and so on. Then the optical image of the FEP film that has been tested as described above is compared to that of the unused FEP, showing only a few differences on the FEP surface after use. And the scanning electron microscopy images (Figure S9a,b, Supporting Information) also indicate the same result. For the rabbit fur, the images in Figure S9c,d (Supporting Information) show the surface of the rabbit fur remains the original scale structure.

2.3. Application of the WLM-TENG

For distributed marine environment monitoring applications, self-powered environmental detection systems based on the water wave energy harvesting were constructed, as illustrated in **Figure 5**a. In such systems, the WLM-TENG working at low frequency converts the mechanical energy of

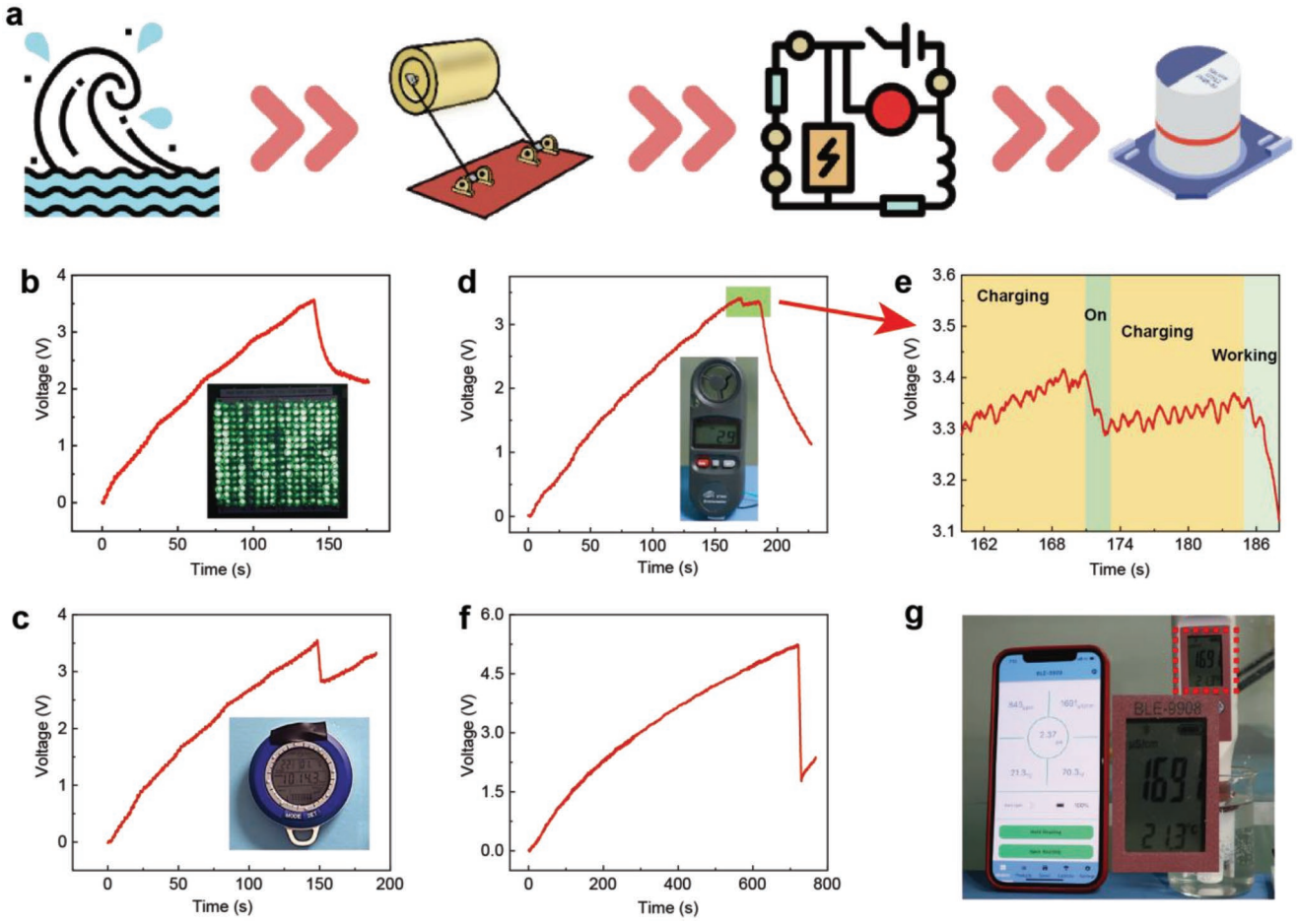

Figure 5. Application of the WLM-TENG in self-powered environmental detection systems. a) Schematic flowchart about the self-powered environmental detection system. b,c) Charging voltage on a capacitor of 3.3 mF when powering 240 LEDs with a diameter of 10 mm and a multifunctional barometer by the power-managed WLM-TENG. The insets show the photographs of the LEDs lighted up and the multifunctional barometer powered. d) Charging and discharging process of the 3.3 mF capacitor when powering a portable anemometer. e) Enlarged view of the voltage profile marked in panel (d). f,g) Voltage curve on a 10 mF capacitor charged by the power-managed WLM-TENG when powering a wireless multifunctional pen of water quality detection, and the photograph of powered detection pen in transmission with a mobile phone.

water wave motion into electrical energy for powering electrical appliances, combined with the power management and energy storage. In this work, around the needs of the marine environment, we have demonstrated the following four applications: LEDs for direction indication, multifunctional barometer, portable anemometer and multifunctional water quality detection pen with Bluetooth transmission function. As shown in Figure 5b, 240 LEDs with a diameter of 10 mm are successfully lighted up by the WLM-TENG integrated with a power management circuit (Video S1, Supporting Information), which can be used as a directional indicator for a shore lighthouse. The voltage profile on the 3.3 mF capacitor is also presented. To detect the atmospheric pressure, a multifunctional barometer was powered by the power-managed WLM-TENG. When the 3.3 mF capacitor was charged to 3.5 V, the switch was turned on to drive the barometer to work normally to obtain local environmental conditions, such as pressure, weather, and temperature, etc. The typical voltage curve on the capacitor and the working process are shown in Figure 5c.

Furthermore, a portable anemometer was also powered by the power-managed WLM-TENG, using a 3.3 mF capacitor as a temporary energy storage unit to supply power (Video S2, Supporting Information). When the capacitor voltage reaches about 3.4 V, the switch of the anemometer is turned on, and the voltage will drop slightly (Figure 5d). A partial enlarged view of the charging curve is shown in Figure 5e. Finally, a multifunctional water quality detection pen with Bluetooth transmission function was used to detect the water-related information, including the temperature of water (TEMP), pH value, total dissolved solids (TDS), and electric conductivity (EC). Here, a 10 mF capacitor was charged to 5.3 V to power the detection pen, exhibiting a typical voltage curve in Figure 5f. Various data about these water-related parameters were wirelessly transmitted through the Bluetooth to the mobile phone apps and displayed on the screen, as shown in Figure 5g and Video S3 (Supporting Information).

3. Conclusion

In summary, a wave-driven cylindrical TENG with a linkage mechanism was fabricated to scavenge the water wave energy. The rotor with unidirectional bearings installed rotates under the enormous wave forces to overcome the great resistance caused by the full contact between rabbit furs and electrodes. The short-circuit current could reach about 30 μA, and the peak power arrives at 50 mW, corresponding to a power density of 14.1 W m^{-3}. Then, a self-powered environmental detection system powered by the WLM-TENG was designed, including four parts: indicating LEDs, multifunctional barometer, portable anemometer and multifunctional water quality detection pen, demonstrating huge potential of the WLM-TENG toward ocean-related applications. This work provides a promising strategy based on the simple mechanical structure to effectively harvest water wave energy, which will find important applications in distributed environmental monitoring.

4. Experimental Section

Fabrication of the WLM-TENG: The 3D printing technology was applied to fabricate the designed WLM-TENG. The shell and rotor were printed by UV-curing resins and polylactic acid plastic, respectively. The inner diameter of the shell was 148 mm, and the thickness of the wall was 3 mm. The outer diameter of the rotor was 146 mm and the depth of the grooves was 10 mm. The central shaft of rotor was supported by ordinary ceramic bearings or one-way bearings to achieve a swing or rotation motion. Commercial rabbit furs with uniform lengths and densities were cut into rectangles (150 mm × 10 mm) by a laser cutting machine. The widths of rabbit furs assembled on rotors with different grids were 4, 10, 20, and 40 mm, respectively. Then double-sided tapes (3 M LSE) were used to attach them on the rotor grooves. For the stator, a piece of copper electrodes (FPC, Flexible Printed Circuit) was divided into different grids (10, 20, 38, and 60 grids), adhered to the inner side of the cylindrical shell. The electrodes were divided into two groups, which were respectively connected. Two wires were led to the edge of the FPC as the output terminals. Then the FEP film was attached on the Cu electrodes for the triboelectrification.

Electric Measurements of the TENG Device: A Keithley 6514 system electrometer was used to test the transferred charge (Q_{SC}) and output current at short-circuit condition (I_{SC}) or the current at a loaded resistance. Then the Keithley 6514 electrometer was used as a voltmeter in series with a high voltage probe (PINTECH HVP-40, 1GΩ) to measure the voltage of the TENG. The performance measurements of fabricated device in simulated water waves were carried out in a regular water tank. A push plate controlled by an actuating motor was employed for generating water waves, and a porous cushion served as the wave absorbing pad for eliminating the rebound waves.

Force Measurement of the Floating Board: A force transducer (SIMBA TOUCH, SBT630) was used to directly test the force applied on the floating board. A signal amplifier (SIMBA TOUCH, RS232485) processed the signals from the force transducer.

Supporting Information

Supporting Information is available from the Wiley Online Library or from the author.

Acknowledgements

J.H. and Y.L. contributed equally to this work. Supports from the National Key R & D Project from Minister of Science and Technology (2021YFA1201604, 2021YFA1201601, and 2021YFA1201603), Innovation Project of Ocean Science and Technology (22-3-3-hygg-18-hy), National Natural Science Foundation of China (Grant Nos. 51432005, 51702018, and 51561145021), and Youth Innovation Promotion Association, CAS are appreciated.

Conflict of Interest

The authors declare no conflict of interest.

Data Availability Statement

The data that support the findings of this study are available from the corresponding author upon reasonable request.

Keywords

blue energy, environmental monitoring, huge driven force, triboelectric nanogenerators, wave-driven linkage mechanism

Received: September 22, 2022
Revised: November 21, 2022
Published online: December 16, 2022

[1] Z. L. Wang, *Nano Energy* **2019**, *58*, 669.
[2] A. D. M. King Mubbert, *Science* **1949**, *109*, 103.
[3] A. M. Omer, *Renewable Sustainable Energy Rev.* **2008**, *12*, 2265.
[4] J. P. Dorian, H. T. Franssen, D. R. Simbeck, *Energy Policy* **2006**, *34*, 1984.
[5] S. A. Montzka, E. J. Dlugokencky, J. H. Butler, *Nature* **2011**, *476*, 43.
[6] L. Jeffry, M. Y. Ong, S. Nomanbhay, M. Mofijur, M. Mubashir, P. L. Show, *Fuel* **2021**, *301*, 121017.
[7] C. McGlade, P. Ekins, *Nature* **2015**, *517*, 187.
[8] S. H. salter, *Nature* **1974**, *249*, 720.
[9] E. Callaway, *Nature* **2007**, *450*, 156.
[10] J. Scruggs, P. Jacob, *Science* **2009**, *323*, 1176.
[11] Z. L. Wang, T. Jiang, L. Xu, *Nano Energy* **2017**, *39*, 9.
[12] A. F. D. O. Falcão, *Renewable Sustainable Energy Rev.* **2010**, *14*, 899.
[13] Z. L. Wang, *Nature* **2017**, *542*, 159.
[14] J. Wang, L. Pan, H. Guo, B. Zhang, R. Zhang, Z. Wu, C. Wu, L. Yang, R. Liao, Z. L. Wang, *Adv. Energy Mater.* **2019**, *9*, 1802892.
[15] L. Xu, T. Jiang, P. Lin, J. J. Shao, C. He, W. Zhong, X. Y. Chen, Z. L. Wang, *ACS Nano* **2018**, *12*, 1849.
[16] Z. L. Wang, *Faraday Discuss.* **2014**, *176*, 447.
[17] Z. L. Wang, *Mater. Today* **2017**, *20*, 74.
[18] Y. Liu, B. Chen, W. Li, L. Zu, W. Tang, Z. L. Wang, *Adv. Funct. Mater.* **2021**, *31*, 2104770.
[19] J. An, Z. M. Wang, T. Jiang, X. Liang, Z. L. Wang, *Adv. Funct. Mater.* **2019**, *29*, 1904867.
[20] C. Zhang, L. He, L. Zhou, O. Yang, W. Yuan, X. Wei, Y. Liu, L. Lu, J. Wang, Z. L. Wang, *Joule* **2021**, *5*, 1613.
[21] X. Liang, T. Jiang, G. Liu, Y. Feng, C. Zhang, Z. L. Wang, *Energy Environ. Sci.* **2020**, *13*, 277.
[22] X. Liang, T. Jiang, Y. Feng, P. Lu, J. An, Z. L. Wang, *Adv. Energy Mater.* **2020**, *10*, 2002123.
[23] X. Liang, Z. Liu, Y. Feng, J. Han, L. Li, J. An, P. Chen, T. Jiang, Z. L. Wang, *Nano Energy* **2021**, *83*, 105836.
[24] T. Jiang, H. Pang, J. An, P. Lu, Y. Feng, X. Liang, W. Zhong, Z. L. Wang, *Adv. Energy Mater.* **2020**, *10*, 2000064.
[25] Z. Lin, B. Zhang, Y. Xie, Z. Wu, J. Yang, Z. L. Wang, *Adv. Funct. Mater.* **2021**, *31*, 2105237.
[26] H. Pang, Y. Feng, J. An, P. Chen, J. Han, T. Jiang, Z. L. Wang, *Adv. Funct. Mater.* **2021**, *31*, 2106398.
[27] Y. Bai, L. Xu, C. He, L. Zhu, X. Yang, T. Jiang, J. Nie, W. Zhong, Z. L. Wang, *Nano Energy* **2019**, *66*, 104117.
[28] Y. Feng, X. Liang, J. An, T. Jiang, Z. L. Wang, *Nano Energy* **2021**, *81*, 105625.
[29] Y. Liu, W. Yan, J. Han, B. Chen, Z. L. Wang, *Adv. Funct. Mater.* **2022**, *32*, 2202964.
[30] L. Long, W. Liu, Z. Wang, W. He, G. Li, Q. Tang, H. Guo, X. Pu, Y. Liu, C. Hu, *Nat. Commun.* **2021**, *12*, 4689.
[31] J. Han, Y. Feng, P. Chen, X. Liang, H. Pang, T. Jiang, Z. L. Wang, *Adv. Funct. Mater.* **2022**, *32*, 2108580.
[32] P. Chen, J. An, S. Shu, R. Cheng, J. Nie, T. Jiang, Z. L. Wang, *Adv. Energy Mater.* **2021**, *11*, 2003066.